Journal of Muscle Research and Cell Motility **1**, 279–303 (1980)

Sinusoidal analysis: a high resolution method for correlating biochemical reactions with physiological processes in activated skeletal muscles of rabbit, frog and crayfish

MASATAKA KAWAI and PHILIP W. BRANDT

Muscle Physiology Division, Departments of Neurology and Anatomy, Columbia University, 630 West 168th Street, New York, New York 10032, U.S.A.

Received 7 January 1980

Summary

A high resolution method for determining the complex stiffness of single muscle fibres is described. In this method the length of the fibre is oscillated sinusoidally, and the resulting force amplitude and phase shift are observed and interpreted in terms of chemo-mechanical energy transduction. In activated, fast skeletal muscles of rabbit (psoas), frog (semitendinosus) and crayfish (walking leg flexor), we resolved at least three exponential rate processes. We named these (A), (B), (C) in order of slow to fast. These processes should reflect ATP hydrolysis and concomitant energy transduction since they are absent in muscles that are relaxed, in rigor or fixed. The great similarities in the complex stiffness data from different muscles suggests that there is a common mechanism of chemo-mechanical energy transduction across a broad phylogenetic range.

Introduction

More than 50 years ago, Fenn (1923) discovered that total energy liberated by a contracting frog sartorius muscle increases in proportion to the work performed. This 'Fenn effect' can be described in terms of contemporary muscle mechanochemistry as a load sensitivity of some rate constants in the actomyosin ATPase cycle, so that crossbridges cycle more rapidly and hence hydrolyse more ATP when more work is done. This load sensitivity, explicitly visualized as the response to strain of individual crossbridges, has been the central assumption of recent work in muscle mechanics. In various forms this strain sensitivity has been incorporated into theories of contraction, to explain force–velocity data (Huxley, 1957; Julian, 1969; Hill, 1974; Hill *et al.*, 1975), oscillatory work (Thorson & White, 1969; Abbott, 1973a), and transient responses to

0142-4319/80/030279-25$04.50/0 © 1980 Chapman and Hall Ltd.

a step change in load (Podolsky & Nolan, 1973) or in length (Huxley & Simmons, 1971; White & Thorson, 1972; Julian *et al.*, 1974; Abbott & Steiger, 1977). Direct experimental measurement of this strain sensitivity is sparse but a form of it was observed in skinned muscle fibres (Kawai & Brandt, 1976), where the dissociation reaction of crossbridges in low levels of MgATP was inhibited or slowed by moderate strain.

There are several physiological techniques in current use which are assumed to depend on the strain sensitivity of the crossbridge reactions. In length–clamp experiments, perturbations in length are related to force changes, while in force–clamp experiments perturbations in force are related to length changes. There are three fundamental wave forms for these perturbations: step, sinusoidal and random noise. We believe that the sinusoidal length perturbation technique maximizes the data obtainable on how modification of the chemical environment alters the crossbridge cycle.

This sinusoidal technique has mostly been employed to observe the phenomenon of 'oscillatory work' in insect muscle (Machin & Pringle, 1959; Pringle, 1967, 1978; White & Thorson, 1973) but has also been used to study other muscle types (Buchthal & Kaiser, 1951; Rack, 1966; Steiger, 1971; Kawai *et al.*, 1977; Kawai, 1978; Saeki *et al.*, 1978). We modified the technique by introducing direct computer control of the length driver and direct access of the computer to both the force and length signals: the wave form of the length change is created in the computer, and amplitude and phase elements are resolved in the programmed digital logic. Our method extends Abbott's (1973b) earlier application, in which he combined a computer with a resolved component indicator (analog device). The time required for measurement is greatly reduced, a wider frequency range can be probed and quantitative analysis of the non-linearity can be made.

Here we describe our technique and emphasize the change in 'complex stiffness' (a frequency response function) of a muscle fibre as it goes through relaxation, activation, rigor and fixation. We also correlate our results with those of the step analysis technique which is at present more commonly employed.

Materials and methods

Reagents

Na_2H_2ATP, H_4EGTA (ethylene glycol-*bis*-(β-amino-ethyl ether) *N,N'*-tetra-acetic acid) were purchased from Sigma Chemical Co. (St. Louis, Missouri); $CaCO_3$, MgO, Mg acetate, propionic acid, NaOH, KOH, imidazole from Fisher Scientific Co. (Pittsburgh, Pennsylvania). The concentrations of multivalent ionic species were calculated after solving the multiple equilibria of two metals (Ca, Mg) and two ligands (EGTA, ATP) by using the apparent association constants as follows (log values at pH 7.00): CaEGTA 6.28, CaATP 3.70, MgATP 4.00. Skinned psoas fibres were relaxed in a saline containing (Na salts in mM) 5 EGTA, 2 MgATP, 7.5 phosphate, 39 sulphate, 43 propionate; activated in 2.4 CaATP, 5 MgATP, 5 free ATP, 7.5 phosphate, 24 sulphate, 43 propionate (pCa 4.1); rigor was induced in 50 sulphate, 47 propionate with several washes. These solutions were buffered with 6 mM imidazole to pH 7.00, ionic strength was maintained at 200 mM, and experiments were carried out at 20° C.

Muscle preparations

Rabbit psoas was prepared as described previously (Reuben *et al.*, 1977; Eastwood *et al.*, 1979). A small fibre bundle tied on a wooden stick was chemically skinned in saline containing (in mM) 5 EGTA, 2 MgATP, 180 K propionate, 5 imidazole (pH 7.00) for 24–48 h at 2° C, as described by Wood *et al.* (1975) for biopsies of human muscle. The preparation was then kept at −20° C in an iso-ionic glycerol–saline (skinning saline + 6 M glycerol). Single fibres were dissected in the skinning saline and mounted in the apparatus for experiments.

Frog (*Rana pipiens*) semitendinosus muscles were dissected in frog control saline (mM: 115 NaCl, 2.5 KCl, 1.8 CaCl, 2 phosphate, pH 7.2) and either the ventral or the dorsal head of the muscle was isolated and used. A small bundle of fibres was tied to a wooden stick and chemically skinned for 4 days at 2° C in saline containing (Na salts in mM) 5 EGTA, 2 MgATP, 40 sulphate, 40 propionate, 7.5 phosphate, 5 imidazole, pH 7.0. Single fibres were isolated for use in the experiments.

A single fibre from the flexor muscle of crayfish (*Orconectes* or *Procambarus*) was dissected (Girardier *et al.*, 1963) in crayfish control saline (mM: 200 NaCl, 5 KCl, 13.5 $CaCl_2$, 5 Tris buffer, pH 7.4). For intact fibre experiments, one end of the fibre was kept attached to the shell membrane and the other to the tendon. When mounted it was held only by the tendon and the shell membrane. For skinned fibre experiments, the sarcolemma was mechanically removed (Reuben *et al.*, 1967, 1971) in the saline containing (in mM) 5 EGTA, 2 MgATP, 170 K propionate, 5 imidazole, pH 7.0, and the fibre mounted between two plastic clamps.

When mounted in the apparatus, the muscle preparations were stretched 10% from slack length (stretched length = L_o), which resulted in a sarcomere length of 2.5–2.6 μm for rabbit psoas, 2.0–2.2 μm for frog semitendinosus and 7–8 μm for crayfish flexor as measured by laser diffraction (wavelength 632.8 nm). At these sarcomere lengths the muscles have practically no resting force or stiffness while when fully activated they develop their maximum force.

Length driver

Details of the length driver and control circuits are shown in Fig. 1a. The length driver consists of two loudspeakers of high compliance (0.13 m in diameter; 40–1284, Tandy Corp., Fort Worth, Texas), and a DC position sensor ('length pickup' in Fig. 1a: 200 DC-B, Schaevitz Engineering, Pennsauken, New Jersey). One speaker is used to drive a stainless steel rod which interconnects all the moving elements including the muscle clamp. The other speaker is used to sense velocity. Since the position sensor has a low frequency response (170 Hz), the velocity signal is integrated to produce position signals at higher frequencies. The two position signals are then hybridized (cross over frequency at 31 Hz) to give a flat response up to 1 kHz. Both velocity and hybridized position signals are fed back to the driving speaker to improve its stability and frequency response (see Machin, 1964, for discussion on feedback theory). Overall response is flat between DC and 200 Hz, and it has a second order roll off with 90° phase shift at 300 Hz. The whole unit is practically free of drift, total excursion is ±1.0 mm, and length change as small as 0.1 μm is possible. It has a low compliance (< 0.05 mm N^{-1}) for externally applied force. A photo-electric position sensor (Photo FET in Fig. 1a) is used for calibration (see Appendix 1) but is not used to control the driver because of drift and gain change.

Force transducer

Two types of transducers were used for this work. One is the Bionix F-100 fitted with a plastic muscle clamp (resonance at 240 Hz; see Fig. 1, Kawai *et al.*, 1977). The other uses strain gauge elements (AE 801; Aker's Micro-Electronics, Horten, Norway; Brandt *et al.*, 1976) to sense the motion of a stainless steel tube connected to the muscle preparation (Fig. 1b). The resonant frequency for this assembly is 2 kHz, and its amplitude can be significantly

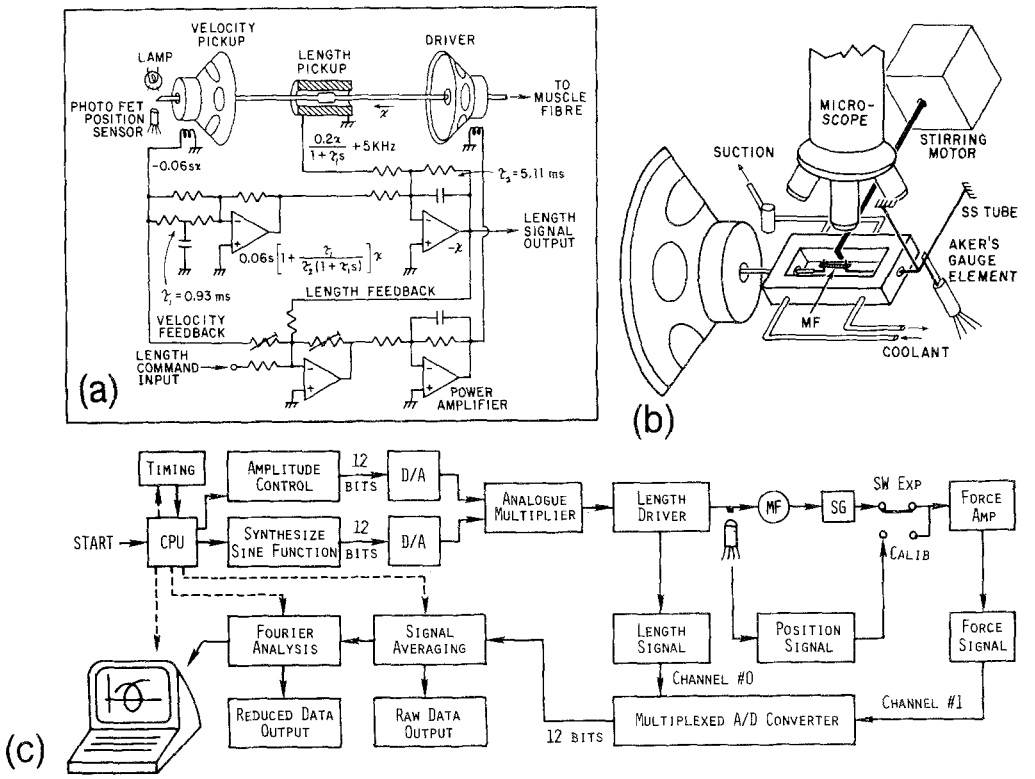

Fig. 1. (a) A diagram of length driver and control circuits (framework only*). Transfer functions are added to the diagram where appropriate. x is a co-ordinate on the driver and s is the Laplace parameter. (b) A sketch of experimental apparatus showing the muscle chamber, strain gauge assembly, a part of the length driver and other accessories. (c) Block diagram of the experiments. Arrows indicate directions of data flow and dotted arrows indicate controls. CPU, central processing unit of a minicomputer; MF, muscle fibre; SG, strain gauge; D/A, digital to analog converter; A/D, analog to digital converter. *Practical details available on request.

damped by application of Vaseline in the gap where the stainless steel tube enters the muscle chamber. Compliance of both transducers is in the range of 0.2–0.4 mm N^{-1}.

Muscle chamber

This is made of an aluminium block (30 mm × 47 mm × 13 mm) with an inside capacity of 0.5 ml. Two stainless steel tubes from the length driver and force transducer assembly respectively enter the chamber through Teflon collars. Although saline does not leak along their gaps a small amount of Vaseline is applied at the other ends of the gaps as extra seals. The aluminium block has a heater coil, a circulation system for cold water and a temperature sensor (not shown in Fig. 1). These are combined together in a feedback network to maintain the block temperature at a desired level (±0.1° C). Saline is constantly stirred to minimize local heterogeneity in solution composition and in temperature. The ends of the muscle preparation are either held in two plastic clamps or wrapped around the stainless steel tubes, then wedged under small clips.

Computer control of length driver

On command a minicomputer (Nova 1220, Data General Co., Southborogh, Massachusetts) synthesizes a series of sine waves via a D/A converter (Fig. 1c). Each sine cycle comprises 8–400 micro steps (Table 1) which are timed by a programmable interval timer. To avoid interference from other peripheral devices the computer interrupt environment is frozen while it controls the length driver and collects data. A second D/A converter is used to set the amplitude of each sine wave (Fig. 1c, Table 1). Outputs of the two converters are multiplied by an analog multiplier (Model 107C, Hybrid Systems Corp.) and fed into the length driver. In this way a flat response (error <1%) at least up to 1 kHz is possible even when the length driver has a lower frequency response. The advantage of this direct control method is the presence of perfect synchronization between the length driver and data collection program, which makes data reduction (signal averaging and/or Fourier analysis) possible during the time of collection.

Data collection and reduction

Both length and force signals are amplified by operational amplifiers to a few volts, then fed into two channels of a multiplexed A/D converter. At the beginning of oscillation at each frequency ≥0.25 s is used to wait for a steady state to be set up before data are collected (longer times were tested without affecting the results). At 100 μs intervals, length and force

Table 1. List of parameters used to control experiments.

Frequency (Hz)	*Amplitude control*	*Interval timer* (ms)	*No. micro steps per cycle*	*Recorded data points per cycle* (m)	*Highest order of harmonics*	*No. cycles* (n)		*Time* (s)	
						Short	*Long*	*Short*	*Long*
714	4.05	0.175	8	8	2	286	1143	0.4	1.6
417	2.30	0.30	8	8	2	167	668	0.4	1.6
250	1.22	0.10	40	8	2	100	400	0.4	1.6
167	1.03	0.15	40	8	2	67	267	0.4	1.6
133	0.97	0.075	100	20	8	54	214	0.4	1.6
100	0.97	0.10	100	20	8	40	160	0.4	1.6
80	0.97	0.12	100	20	8	32	128	0.4	1.6
50	0.98	0.10	200	40	18	20	80	0.4	1.6
33.3	0.99	0.15	200	40	18	14	54	0.42	1.6
25	1.00	0.10	400	40	18	10	40	0.4	1.6
16.7	1.00	0.15	400	40	18	7	27	0.42	1.6
10	1.00	0.25	400	40	18	4	16	0.4	1.6
7.14	1.00	0.35	400	40	18	3	12	0.42	1.6
5	1.00	0.50	400	40	18	2	8	0.4	1.6
3.13	1.00	0.80	400	40	18	2	5	0.64	1.6
2	1.00	1.25	400	40	18	1	4	0.5	2
1	1.00	2.50	400	40	18	1	2	1	2
0.5	1.00	5.00	400	40	18	1	1	2	2
0.25	1.00	10.00	400	40	18	1	1	4	4

For the current report, only frequencies ≤ 167 Hz are used. Higher frequencies are used for calibration curves of Fig. 9.

signals are sampled and added to the previously accumulated samples at the same respective position in the cycle. Thus 8–40 points (depending on frequency; Table 1) represent the time course of the signal averaged cycle. Data are accumulated for the n cycles (Table 1) needed to obtain a duration which just exceeds 0.4 s (short time course) or 1.6 s (long time course). As soon as the data are collected the length driver is stopped and the data are expanded into Fourier series:

$$P(t,f) = \sum_{k=-\infty}^{\infty} P_k(f) \exp(2\pi ikft)$$

where

$$P_k(f) = f/n \int_0^{n/f} P(t,f) \exp(-2\pi ikft)\, dt \quad (1)$$

and f is frequency of oscillation, t is time, $P(t,f)$ is periodic force time course. The term corresponding to $k = 0$ represents the average force, $k = \pm 1$ represents the linear component and $k = \pm 2, \pm 3, \pm 4, \ldots$ represent harmonic components.

Complex stiffness $Y(f)$ is a frequency response function of the muscle relating force to length changes: $Y(f) = P_1(f)/L_1(f)$, where $L_1(f)$ is obtained similarly to equation 1 from periodic length time course data. The complex stiffness represents ratio of amplitudes of force to length (hence 'stiffness') by $|Y(f)|$, and phase shift between force and length sine waves by $\arg[Y(f)]$. Data are standardized with the size of the preparation when this information is reliable: $Y_M(f) = Y(f) \cdot L_0/A_0$, where L_0 is the length of the muscle preparation, and A_0 is its cross-sectional area. $Y_M(f)$ is called the 'complex modulus', its real part is called the 'elastic modulus' and the imaginary part the 'viscous modulus'. L_0 is measured through a dissecting microscope with an ocular micrometer and the diameter through a compound microscope (400 ×). Cylindrical shape is assumed in order to calculate the cross-sectional area; this calculation was only performed for single fibres of rabbit psoas. The unit of stiffness is N m^{-1} and of modulus is N m^{-2}.

Total elapsed time to collect data at 16 frequencies (0.25–167 Hz) is 22 s, including waiting periods for steady state, complex stiffness calculation and storage of the results in a disc file. Two seconds later the reduced data are displayed as a Nyquist plot and as frequency plots. This display is used to judge the quality of the data, the condition of the muscle preparation and the condition of the overall experimental system. The data thus collected are corrected for the system response; appendix 1 details the correction procedure.

Results

Rabbit muscle

Chemically-skinned rabbit psoas fibres were first washed in a relaxing saline, then transferred to an activating saline, washed with rigor saline several times to induce the 'high rigor' state (Kawai & Brandt, 1976) and relaxed again. Fig. 2 illustrates a series of length and tension time courses recorded in two of these conditions; Lissajous figures are also shown. In activated muscle the Lissajous figures rotate clockwise in the high and low frequency ranges while they rotate counter-clockwise at medium frequencies (shaded). This means that the fibre absorbs work from the oscillating length driver in the high and low frequency ranges, while it generates 'oscillatory' work at medium

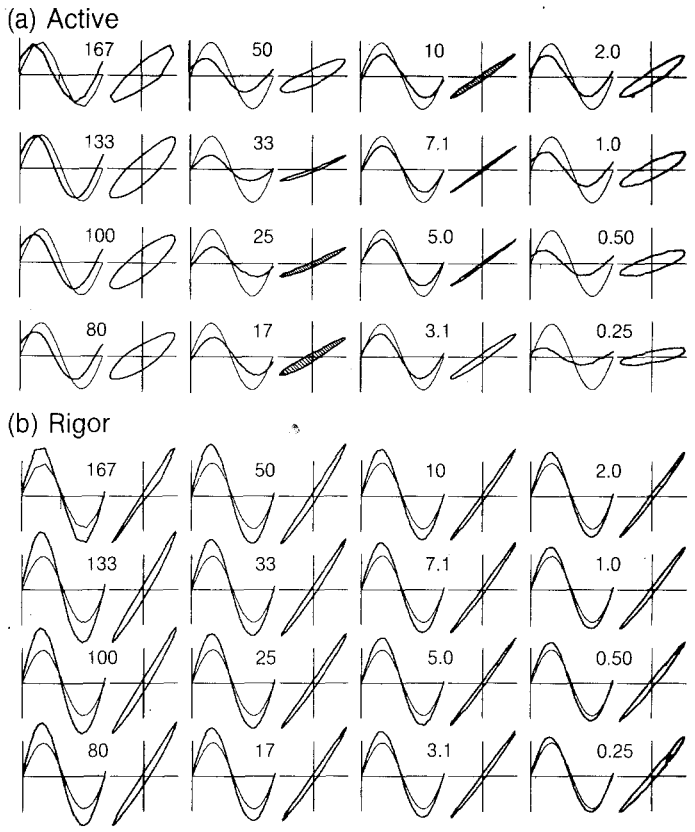

Fig. 2. Raw data collected from chemically skinned rabbit psoas during activation (a), and rigor (b) at 16 frequencies (Hz). Each record constitutes a length (thin line) and force (thick line) time course and Lissajous figure. 8–40 points (Table 1) were collected per curve and these are connected by straight lines. The full length of the axes corresponds to 10 μm or 120 μN. Peak–peak amplitude change: 0.23%L_0. Each time scale is adjusted so that only one averaged cycle is displayed. For the purpose of display, drift during measurement is subtracted.

frequencies. This work is *net work*, the difference between the work performed by the muscle during the shortening phase and by the driver during the lengthening phase. The shaded area enclosed by the Lissajous loop is proportional to the amount of mechanical energy produced per cycle of length oscillation. Oscillatory work is absent when fibres in the high rigor state are studied (Fig. 2b). In this condition the Lissajous figures are least sensitive to frequency changes, and small amounts of energy are absorbed by them.

Fig. 3 shows complex modulus data taken from Fig. 2 for activated and rigor conditions and the data from the relaxed fibres are also included. The complex modulus data are relatively simple and constant for relaxed or rigor muscles. At L_0 relaxed muscle is least stiff and points scatter around the origin of the Nyquist plot

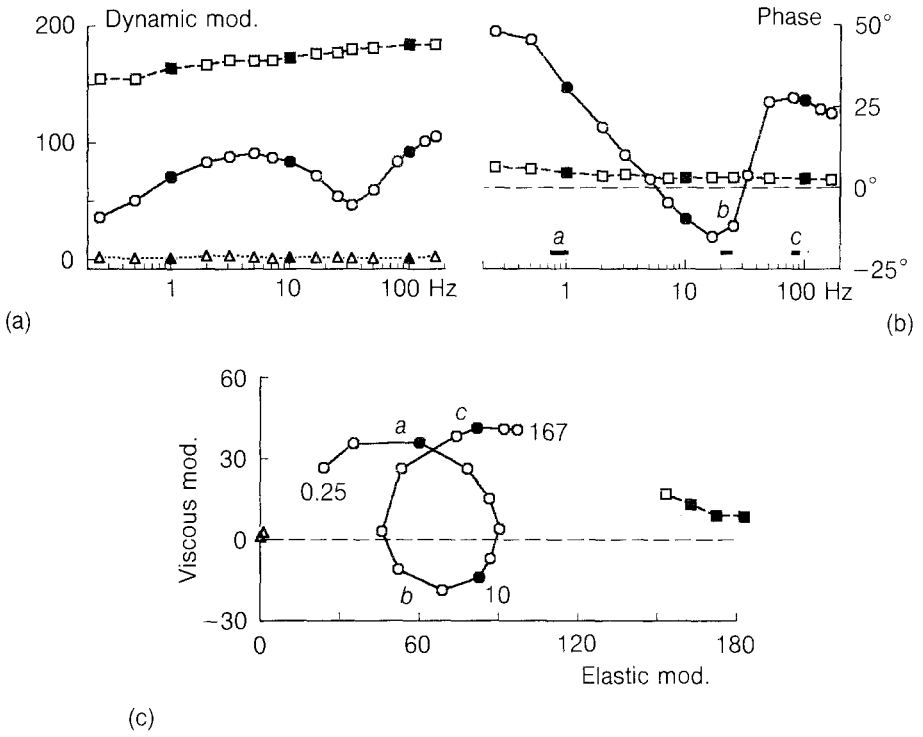

Fig. 3. Plots of complex modulus $Y_M(f)$ of rabbit psoas during relaxation (© . . . △), activation (○——○), and high rigor (□----□). Unit of moduli is 10^5 N m^{-2}. Activated and rigor data are derived from Fig. 2. Some of the frequency points are omitted from the plots for simplicity, and the filled symbols correspond to decade frequencies (1, 10, 100 Hz). In (b), horizontal bars along frequency axis (abscissa) indicate characteristic frequencies *a*, *b*, *c* and their 95% confidence ranges. Phase of relaxed muscle is indeterminate and not entered here. In (c), approximate locations of characteristic frequencies are marked, and the numbers around data points correspond to frequency. Isometric force was 1.35×10^5 Nm^{-1}.

(Fig. 3c). Rigor muscle is most stiff and there is a weak frequency dependence (Fig. 3a, b). The dynamic modulus is slightly higher at high frequencies and the phase shift is minimal (an advance: 4–5° before correction, 2–3° after correction). This tendency of the complex modulus is true of all the muscle types we studied. The rigor muscle's high elasticity and low viscosity approximate an elastic material. The Nyquist plot of activated muscles is trifoliate (Fig. 3c). There is a point of crossover where both amplitude and phase are the same for two different frequencies. This point divides the plot into three arcs.

Data analysis

Since an exponential process is represented in a Nyquist plot by one hemicircle with its centre on the abscissa (see Machin, 1964), the presence of three arcs is compatible

with the existence of three exponential processes in the length to force relationship. We name the respective processes (A), (B), (C) in the order of slow to fast. Process (A) is a low frequency-exponential advance, and centres around 1 Hz where the muscle absorbs net work from the length driver. Process (B) is a medium frequency-exponential delay centering around 17 Hz and the muscle generates oscillatory work. Process (C) is a high frequency-exponential advance centred at around 100 Hz and again the muscle absorbs work.

The data for activated fibres can be approximated by a transfer function of the sum of three exponential rate processes:

$$\begin{matrix} & & \text{Process (A)} & & \text{Process (B)} & & \text{Process (C)} \\ Y_M(f) = H + & \dfrac{Aif}{(a + if)} & - & \dfrac{Bif}{(b + if)} & + & \dfrac{Cif}{(c + if)} \end{matrix} \qquad (2)$$

where A, B, C are magnitude parameters, a, b, c are characteristic frequencies of processes (A), (B), (C) respectively, and H is the elastic modulus at DC. Mechanical equivalence of equation 2 is depicted in Fig. 7c. The data are fitted to equation 2 by a least squares method in order to obtain magnitude and frequency parameters. The fitting procedure is complicated because equation 2 is non-linear with respect to the characteristic frequencies. A description of such a procedure is given in Appendix 2. Fig. 7a is a Nyquist plot which is the result of fitting the data of Fig. 3 to equation 2. We also calculate the 95% confidence range for the fitted parameters (Appendix 2). Usually the range is about ±15% for frequency parameters a, b and c (entered in Fig. 3b). Although we do not imply that complex stiffness of activated muscle is perfectly represented by equation 2, it is a good approximation of the data in the present frequency range as shown by the narrow confidence limits. Obviously the data would fit better to transfer functions which incorporate more rate processes at higher frequency ranges which we should consider when the frequency range is extended in the future (cf. Abbott & Steiger, 1977; Ford *et al.*, 1977).

Comparison of rabbit psoas with other muscle preparations

To discover whether other fast skeletal muscles have similar properties to those of skinned rabbit psoas fibres, the flexor muscle of crayfish walking legs and the semitendinosus muscle of frog were tested before and after disruption of the sarcolemma (skinning). Raw data from an intact crayfish fibre is displayed in Fig. 4, and Fig. 5 shows Nyquist plots from all preparations. Fig. 5a is obtained from a single fibre of crayfish activated by elevating the K^+ concentration in the bathing saline. Fig. 5b is from frog semitendinosus muscle in a caffeine contracture. Fig. 5c, d respectively represent a mechanically-skinned single fibre of crayfish and a chemically-skinned single fibre of frog semitendinosus. Both were activated by high Ca and high MgATP solutions. All three processes (A), (B), (C) are present as labelled in the figure. Significantly, oscillatory work previously associated with insect muscles is manifest in all the fast striated muscle preparations we studied.

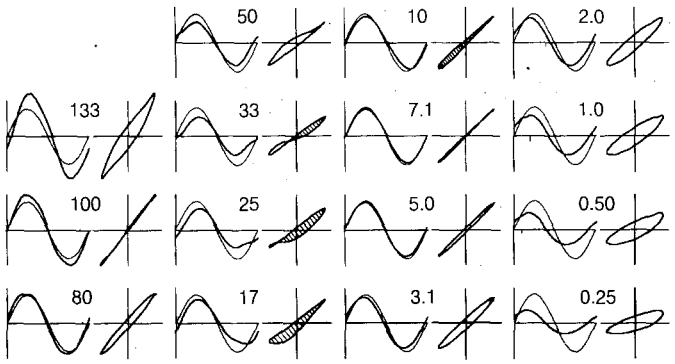

Fig. 4. Raw data obtained from intact crayfish single muscle fibre during K activation (200 K propionate, 5 imidazole, pH 7.0, 20° C). See Kawai *et al.* (1977) for details of activating conditions, and legend of Fig. 2 for conventions. Full length of axes corresponds to 16 μm or 6 mN. Peak–peak length change: 0.27%L_0. Because these data were obtained with our original equipment when a carrier amplifier (low frequency response), Bionix F100 strain gauge, and plastic muscle clamps were in use, data at the higher frequency are contaminated with phase delay artifacts. This error is compensated for (Appendix I) in the Nyquist plot of Fig. 5a by use of curve 5 of Fig. 9d.

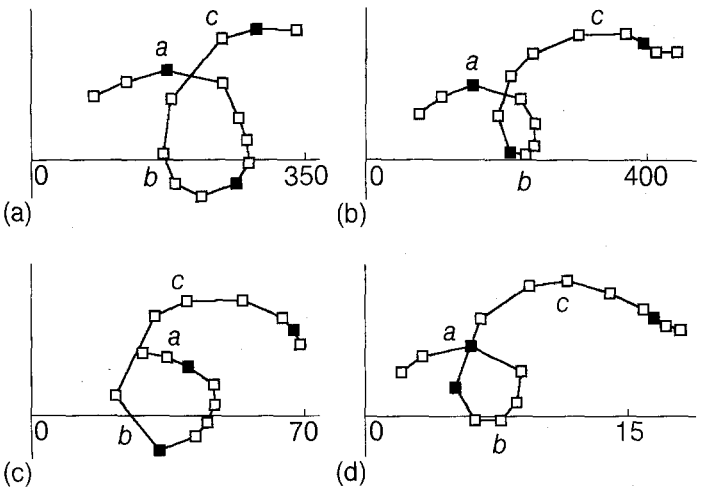

Fig. 5. Nyquist plots during activation. Plots of complex stiffness $Y(f)$. (a) Intact crayfish single muscle fibre with K activation (for conditions see legend of Fig. 4 from which this data was derived). (b) Intact frog semi-tendinosus muscle (one head) with caffeine activation [20 Caffeine, 115 NaCl, 2.5 KCl, 1.8 $CaCl_2$, 2 Na propionate, pH 7.2, 10° C]. (c) Mechanically skinned crayfish single fibre activated by a pCa 3.8 solution [(Na salts) 17.2 MgATP, 2.86 CaATP, 2.92 ATP, 3.5 phosphate, 88 K propionate, 5 imidazole, pH 7.00, 20° C]. (d) Chemically skinned frog semitendinosus single fibre activated by pCa 3.9 solution [(Na salts) 2.5 CaATP, 2 MgATP, 5 ATP, 7.5 phosphate, 28 sulphate, 13 propionate, 50 imidazole, pH 6.75, 10° C]. Approximate locations of characteristic frequencies (a, b, c) are indicated in each figure. The abscissae indicate units of stiffness in N m^{-1}. Isometric force was 20, 72, 5.4, 0.86 mN; length was 4.8, 18, 4.4, 3.0 mm in the order (a)–(d) respectively.

Analysis for non-linearity

By visual examination of Fig. 2b it is clear that the sinusoidal waveform of the force time courses of rigor muscle is minimally distorted and that the corresponding Lissajous loop is elliptic in appearance. In active fibres, however, there is some distortion in the frequency range where the oscillatory work is prominent (Figs. 2a, 4). Quantitative analysis for non-linearity is carried out by estimating the magnitude of the harmonics in the waveform of the force time course. From equation 1 the relative amplitude of the kth harmonic is calculated by:

$$h_k(f) = |P_k(f)|/\sqrt{I(f)} \tag{3}$$

where $k = 1, 2, 3, \ldots$; $h_1(f)$ is linearity, and $I(f)$ is half the oscillation power:

$$I(f) = \sum_{k=1}^{\infty} |P_k(f)|^2 = \frac{f}{2n} \int_0^{n/f} [P(t,f) - P_0]^2 \, dt$$

P_0 is the average force. Theoretically we should be able to calculate harmonics up to half the number (m) of the data points in a cycle (Nyquist frequency; see Bendat & Piersol, 1971), but in our experience we can only calculate $m/2 - 2$. The highest practical order of harmonics is shown in Table 1. Distortion (non-linearity) is calculated by:

$$D(f) = \sqrt{\sum_{k=2}^{\infty} |h_k(f)|^2} = \sqrt{[1 - h_1(f)^2]} \tag{4}$$

The results of calculations of non-linearity in data from activated muscle preparations are summarized in Fig. 6. Only terms corresponding to $D(f)$, $h_1(f)$, $h_2(f)$, $h_3(f)$, $h_4(f)$ are shown since higher order terms vanish rapidly. Fig. 6a was obtained from chemically-skinned rabbit psoas (data from Fig. 2a); Fig. 6b from intact crayfish flexor (from Fig. 4). As shown in Fig. 6 most of the non-linearity is explained by the 2nd order harmonic modulation and amplitudes are progressively less for the 3rd and 4th order terms. In rabbit psoas when the peak–peak length oscillation is 0.23% L_0, the distortion does not exceed 0.11 so that the non-linear power is $\leqslant$1.2%, and linearity is $\geqslant$ 0.994. The non-linear profiles in activated rabbit psoas and crayfish muscles are strikingly similar although distortion is larger in the latter. Relatively larger non-linearity, evident at frequencies around oscillatory work [process (B)], peaks approximately at the frequency where the dynamic modulus becomes a minimum (cf. Figs. 3a and 6a). This frequency is slightly higher than the characteristic frequency b.

Distortion associated with processes (A) and (C) is smaller. In Fig. 6a this amounts to 0.06 with a corresponding linearity of 0.998. Distortion for rigor or fixed muscle is likewise small and we obtained 0.04 for the data in Fig. 2b. When the same analysis is carried out on a blank (no muscle), we usually find that $D(f) > 0.9$ with corresponding amplitude of 1 μN. This is due to instrumental noise and the value indicates a limit to

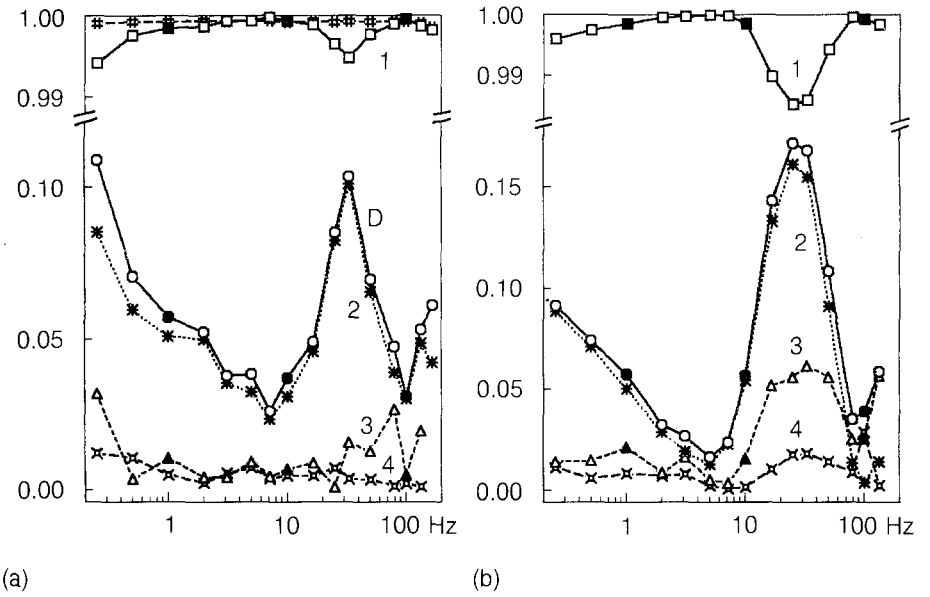

Fig. 6. Plot of relative harmonic amplitudes $h_k(f)$ (terms corresponding to k = 1, 2, 3, 4 are labelled) and distortion $D(f)$. Curve 1 represents linearity, and curve D represents distortion (non-linearity). Note breaks in the ordinates. (a) Data derived from Fig. 2a (activated psoas) except for the top curve (--#) which was derived from Fig. 2b (rigor). (b) Data derived from Fig. 4 (activated crayfish muscle).

our measurements. This limit indicates that we are able to detect periodic deflection of the strain gauge by 0.2 nm, since its compliance is 0.2 mm N^{-1}.

Discussion

Non-linearity in force time course

Calculation of $P_1(f)$ by means of the Fourier integral (equation 1) corresponds to fitting a periodic force time course $P(t, f)$ to sine and cosine functions of the same periodicity. This is in essence a linear regression method involving three fitting parameters. We assess goodness of fit, therefore, by evaluating the regression coefficient which in our case is equivalent to the linearity h_1 (equation 3; curve 1 in Fig. 6). It is 0.994 for the worst case in the data of Fig. 2a, and 0.985 in the data of Fig. 4. Thus it is apparent that the force response is so linear that its time course is described adequately by sine and cosine functions of the same periodicity, which validates the present sinusoidal analysis technique as applied to muscle systems.

The very high linearity ($\geq$ 0.998; Fig. 6a) associated with process (C) is unexpected from the results of step length change experiments. Huxley & Simmons (1971) reported severe asymmetries in their rate constant measurements of 'phase 2', which corresponds to process (C) (see below); the rate constant is faster on release and

slower on stretch in intact frog semitendinosus preparations. Similar asymmetries are observed in other muscle types (Heinl *et al.*, 1974; Abbott & Steiger, 1977). Although a general qualitative conversion method which relates a non-linearity in the sinusoidal analysis to asymmetry in the step analysis technique is not available at hand (unless a model is involved), it appears that the non-linearity observed in process (C) is much smaller than would have been anticipated from the step analysis experiments. We are forced to conclude, therefore, that the muscle responds more linearly to a sinusoidal length change than to a step change.

Although we can only speculate on the immediate cause of this discrepancy, an observation of Sugi & Tameyasu (1979) may be relevant (see also Sugi, 1979). They discovered by ultra high speed cinematography that with a quick length release their semitendinosus preparation buckled at the released end. Such buckling, which perturbs the tension signal, could account for the discrepancy. It would be useful to combine high speed cinematography with measurements of force transients. The basis for the linearity/asymmetry may not be clarified until we are much closer to an understanding of the transduction process, but obviously it is important to use several techniques and to compare their respective results. No one method can be considered as certain in such a complex system.

The relatively large non-linearity associated with process (B) (oscillatory work) is striking, although the corresponding linearity is still 0.994 (psoas), representing a degree of non-linearity not serious enough to distort our measurements. This is seen in both rabbit and crayfish preparations (Fig. 6). The maximum non-linearity takes place approximately at the frequency at which the dynamic modulus is minimal (cf. Figs. 3a and 6a), a frequency slightly higher than the optimal frequency for oscillatory work. At this frequency the force signal is most distorted, presumably because the crossbridge stroke interferes with the length driver most significantly. Steiger (1971) observed larger distortion in sinewaves associated with oscillatory work in freeze-dried cardiac preparations (see also White & Thorson, 1972; Abbott, 1973a). It is possible that the distortion is associated with irreversible reactions such as hydrolysis of MgATP and oscillatory work production.

Correlation of rate processes with force transients

It is useful to correlate the 'rate processes' we observe in sinusoidal analysis to the 'stages' (Huxley & Simmons, 1971) or 'phases' (Huxley, 1974) of step analysis. The correlation is graphically presented in Fig. 7a, b which is qualitatively derived as follows. We set $s = 2\pi fi$ (s is the Laplace parameter) and rewrite equation 2:

$$Y(s) = H + \frac{As}{(2\pi a + s)} - \frac{Bs}{(2\pi b + s)} + \frac{Cs}{(2\pi c + s)}$$

In transient studies, force change relates to length change by

$$\Delta P(s) = Y(s)\,\Delta L(s)$$

where $\Delta L(s)$ and $\Delta P(s)$ are Laplace transforms of the length and force deviation time courses $\Delta L(t)$ and $\Delta P(t)$ respectively. For a step length change of the size δl, $\Delta L(s) = \delta l/s$. By substituting this in the above equations, we obtain

$$\Delta P(s) = \left[\frac{H}{s} + \frac{A}{(2\pi a + s)} - \frac{B}{(2\pi b + s)} + \frac{C}{(2\pi c + s)}\right] \delta l$$

By performing an inverse Laplace transform, the force time course is (for $t > 0$):

$$\Delta P(t) = [\underbrace{C \exp(-2\pi ct)}_{\text{(Phase 2)}} - \underbrace{B \exp(-2\pi bt)}_{\text{(Phase 3)}} + \underbrace{A \exp(-2\pi at)}_{\text{(Phase 4)}} + H]\, \delta l \qquad (5)$$

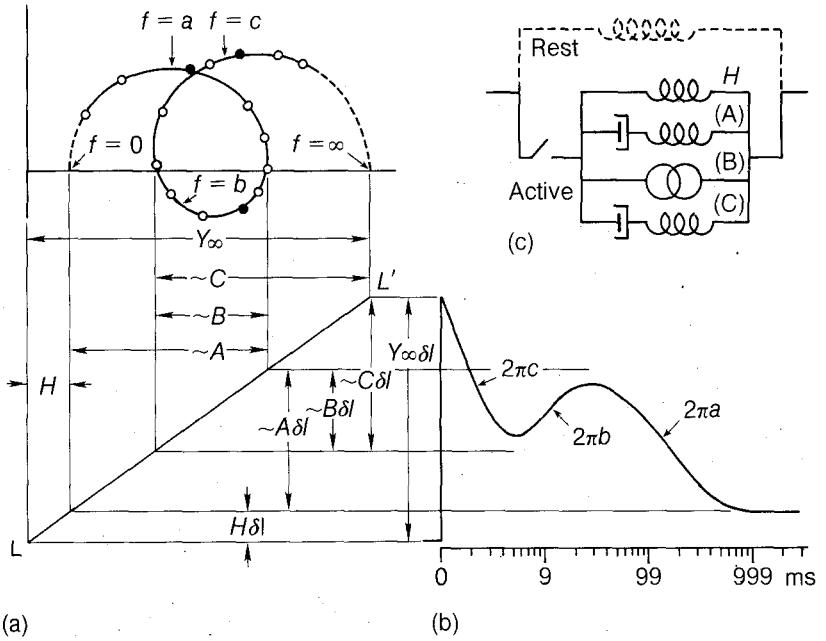

Fig. 7. Correlation between sinusoidal (a) and step (b) analyses and equivalent diagram (c). (a) Theoretical curve to describe complex modulus data of an active muscle is represented in a Nyquist plot. The curve and points (corresponding to our experimental frequencies) are calculated by using equation 2 with best fit parameters to a curve of Fig. 3: $a = 0.87$; $b = 21.9$, $c = 83.8$ (unit in s^{-1}); $H = 15.1$, $A = 80.8$, $B = 86.3$, $C = 118$ (unit in 10^5 N m^{-2}). Approximate magnitude or position of these parameters are indicated. f, frequency. (b) Simulated force time course following a step length increase. The data are calculated using equation 5 with the same parameters used to construct (a). Rate constants of each phase are indicated by arrows. Note logarithmic time scale. Diagonal line LL' symbolizes the inverse Laplace transformation. (c) Equivalent mechanical diagram to explain three rate processes (A), (B), (C) and the constant H of equations 2 and 5. Expression of the process (B) is tentative. Resting component is almost negligible.

The equation is rearranged in the order of fast to slow. From equation 5 the following time course is predicted (Fig. 7b). On step length increase ($\delta l > 0$) at $t = 0$, there is a simultaneous increase in force corresponding to $Y_\infty \delta l$, where $Y_\infty = H + A - B + C$, which is equivalent to phase 1. Then there is a *fast relaxation* of the force with a rate constant of $2\pi c$. This corresponds to phase 2 and magnitude of $\sim C\delta l$. This is followed by a *reversal* of the force with an exponential rate constant of $2\pi b$ and magnitude of $\sim B\delta l$. This part of the force is often called 'delayed tension' and corresponds to phase 3. In most data reported on frog muscle (for example, Huxley & Simmons, 1971) this phase exhibits a plateau (their earlier abstract shows a 'delayed tension'; Armstrong *et al.*, 1966), because delayed tension is less evident in the step method since it is bounded by two exponentially decaying time courses. This is clearly shown in Fig. 7b as smaller delayed rise in force than projected from the Nyquist plot of Fig. 7a. In the sinusoidal method we unambiguously observed process (B) in both intact and skinned frog preparations (Fig. 5b, d).

After the delayed tension, the force once again changes its direction and *relaxes* exponentially with a slow rate constant of $2\pi a$. This corresponds to phase 4, and its magnitude is $\sim A\delta l$. The final force level is *slightly higher* than before the length increase, and corresponds to $H\delta l$ (cf. Sugi, 1972; Edman *et al.*, 1976; Hill, 1977). We always find $H > 0$, although it is small compared to the other parameters. It should be clear in the foregoing discussion that the rate constants are obtained by multiplication of the characteristic frequencies a, b, c by 2π (see also Pringle, 1978). This factor 2π must not be forgotten when comparing the limits of resolution of the sinusoidal and step methods: if the highest resolved frequency is 167 Hz, then the limit of time resolution is 1 ms and not 6 ms.

In this correlation the polarity of process (B) (phase 3) allows it to be identified unambiguously because its polarity is unique (negative). We define process (C) (phase 2) as the one faster than (B), and process (A) (phase 4) as that slower than (B). Whereas we resolve only one process between DC and (B), there may be more than one process between (B) and infinite frequency (Abbott & Steiger, 1977; Ford *et al.*, 1977). This method of identification and correlation of each process or phase is useful when various muscle preparations are to be compared under numerous experimental conditions, since process (B) is universally present in all preparations studied so far. Table 2 summarizes the correlations between the various reports. The present rate processes apparently relate to 'length transients' observed in force step experiments (Podolsky, 1960; Civan & Podolsky, 1969; Podolsky *et al.*, 1974); see Huxley (1974) for the correlation between length and force transients.

The above correlation is qualitatively valid when (i) a system is linear and (ii) the property of the system is unaffected by the length change. Although these are difficult conditions to meet in a muscle system, we can assume that the system behaves so when the length change is infinitesimally small. In fact we satisfy the linearity requirement when the peak–peak length change is about 0.2–0.3%L_0 (see p. 290). At larger amplitudes we have to extrapolate the above correlations and therefore the

Table 2. Correlation of the processes and phases from various laboratories.

Name	*Kawai* et al. *(1977); Kawai (1978, 1979); this report*	*Huxley (1974); Heinl* et al. *(1974); Ford* et al. *(1977)*	*Abbot & Steiger (1977)*	*Other reports*
Instantaneous stiffness	Y_∞	Phase 1	Phase 0	Huxley & Simmons (1971, 1973)
High frequency phase advance	Process (C) R.C. = $2\pi c$	Phase 2	Phases 1, 2 R.C. = K_1, K_2	Huxley & Simmons (1971); Thorson & White (1969); Abbott (1972)
Oscillatory work (phase delay)	Process (B) R.C. = $2\pi b$	Phase 3	Phase 3 R.C. = K_3	Machin & Pringle (1959); Pringle (1967, 1978); White & Thorson (1973)
Low frequency phase advance	Process (A) R.C. = $2\pi a$	Phase 4	Phase 4 R.C. = K_4	Hill (1953); Gasser & Hill (1924)
Residual (DC) stiffness	H			Sugi, H. (1972); Edman *et al.* (1976); Hill (1977); Amemiya *et al.* (1979)

R.C., rate constant.

correlation becomes qualitative. Even so the polarities and the speed of the processes which are used to map our processes to phases of Huxley (1974) remains the same.

Interpretation of the rate processes in terms of mechanochemistry

Our objective is to map empirically the apparent rate processes to intrinsic chemical reactions in a crossbridge cycle scheme (e.g. Lymn & Taylor, 1971; Trentham *et al.*, 1976; Stein *et al.*, 1979). This mapping can be carried out by changing an experimental condition which is known to alter a particular chemical reaction and by following the change in the rate processes. Simple experiments include the elimination of substrate (MgATP) or Ca ions. Processes (A), (B) and (C) are present in a fully active muscle but they are absent in a rigor or relaxed muscle. This is convincing evidence that these three rate processes are fundamental properties of cycling crossbridges. The fact that all of them are present in a variety of fast striated muscle tissues leads us to suggest that they are fundamental properties of the transduction mechanism.

We reported earlier (Kawai & Brandt, 1975, 1979; Kawai & Orentlicher, 1976; Kawai, 1978, 1979) that physiological concentrations of MgATP can limit the rate processes (B) and (C) in both crayfish and rabbit systems. We use this observation as evidence that MgATP binding to rigor-like actomyosin linkage and subsequent dissociation are represented in processes (B) and (C). Evidently (B) is oscillatory work and since one actually detects a maximum in mechanical energy production which is correlated with ATPase rate (Rüegg & Tregear, 1966; Steiger & Rüegg, 1969; Pybus & Tregear, 1975) a maximum in the number of transduction steps must occur at around frequency b. It seems that phosphate greatly affects process (B), but not (C) (Kawai & Orentlicher, 1976) indicating that (C) is not limited by the particular energy transduction transition. The phosphate effect is, however, opposite from expectation and further clarification is needed (cf. White & Thorson, 1972). Process (A) is related to the force recovery phase earlier studied by Hill (1953), although he used a bigger length release (about 5%) and therefore the phenomena are not necessarily identical. We find that this process is least sensitive to factors such as physiological concentration of MgATP, phosphate, temperature, etc. and we conclude that process (A) is not limited by these factors.

Appendix 1

Method of correcting complex stiffness data

There are two classes of systematic errors (type I, II) which can be removed from the data by appropriate corrections. We use complex number nomenclature to quantify these errors since it is easier to handle them in the frequency domain. Type I error is associated with the electronics; it arises in the magnetic-electric position sensor, force amplifier and from the use of a multiplexed A/D converter for the length and force signals (Fig. 1c). Type I error is represented by $E(f)$. Type II error arises in the mechanics of the force transducer assembly, which includes the strain gauge element, muscle clamp, Vaseline seal, and lever connecting the gauge to the clamp (Fig. 1b). This error is represented by $g(f)$. Mass, viscosity and elasticity are the important parameters governing $g(f)$.

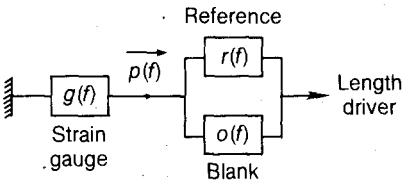

Fig. 8. Mechanical arrangement of system calibration. $g(f)$, $r(f)$, $o(f)$ represent true complex stiffness of strain gauge, reference and blank respectively.

In order to quantify type I error, a photo field-effect transistor (Photo FET in Fig. 1a: FF600, Teledyne Crystalonics, Cambridge, Massachusetts) is used to observe the performance of the length driver ('position signal', Fig. 1a, c). Output of the transistor is fed into the force amplifier (SW in Fig. 1c is connected to 'calib' side), and a frequency response function $E(f)$ is collected in the usual manner. In this way all type I errors are lumped together in $E(f)$. It is displayed in Fig. 9c, d for our original equipment (curve 5), and for our most recent equipment (curve 6).

We have to obtain $g(f)$ at each frequency in order to compensate for type II errors rather than determining mass, viscosity and elasticity of force transducer assembly (cf. Ford *et al.*, 1977). In our case, the type II error is not described in a simple second order differential equation since (a) the lever connected to the strain gauge has a complicated bending motion and (b) the interaction between the Vaseline seal and the stainless steel rod is in no way first order. Instead we determine $g(f)$ by a measurement at each frequency.

In order to obtain $g(f)$ we need a reference material whose true complex stiffness $r(f)$ is known. It is best if $r(f)$ is constant with frequency but this is not a requirement. The reference material is mounted in the apparatus and complex stiffness is measured in the usual manner. The measured complex stiffness $R(f)$ is related to $r(f)$ by:

$$R(f) = E(f)\frac{g(0)[r(f) + o(f)]}{g(f) + r(f) + o(f)} \tag{6}$$

where $o(f)$ represents blank coupling between the length driver and the strain gauge. Equation 6 is derived from the fact that $r(f)$ and $o(f)$ are parallel to each other, and that they are connected serially to $g(f)$ (Fig. 8). $g(0)$ is the DC stiffness of the strain gauge and must be measured independently [$|g(1\text{ Hz})|$ is used for this purpose]. $g(0)$ appears in equation 6 because the force is sensed after multiplication of this parameter with the displacement of the gauge lever. In the frequency domain the true force $p(f)$ and observed force $P(f)$ are related by

$$p(f) = [g(f)/g(0)]P(f)$$

since the strain gauge is a displacement sensor.

The measurement is repeated after the reference material is removed. This is to assess the true blank coupling $o(f)$ which arises from resonance of table and standing waves on the surface of the saline. By setting $r(f) = 0$ in equation 6, measured blank coupling $O(f)$ is:

$$O(f) = E(f)g(0)o(f)/[g(f) + o(f)] \tag{7}$$

From equations 6 and 7 we can solve for $g(f)$ and $o(f)$.

$$g(f) = [g(0)E(f) - O(f)]\left\{\frac{r(f)[E(f) - R(f)/g(0)]}{E(f)[R(f) - O(f)]}\right\}$$

$$o(f) = O(f)\left\{\frac{r(f)[E(f) - R(f)/g(0)]}{E(f)[R(f) - O(f)]}\right\}$$

Once $g(f)$ and $o(f)$ are known, measured complex stiffness $Y(f)$ relates to correct $y(f)$ by (cf. equation 6)

$$Y(f) = E(f)g(0)[y(f) + o(f)]/[g(f) + y(f) + o(f)].$$

Solving this for $y(f)$ we get

$$y(f) = g(f)Y(f)/[g(0)E(f) - Y(f)] - o(f)$$

This corrected form of the complex stiffness is used in all of our reports.

For reference material we used fixed muscle, first bringing a fibre into the high rigor condition (Kawai & Brandt, 1976), then treating it with 2.5% glutaraldehyde for ≥ 5 min (half fix time is ~ 1 min, judged by stiffness time course). We find this material to be more suitable (less viscous, lighter) than a rubber band, a spring or a thin steel wire. Normalized frequency response $r(f)/r(0)$ of fixed muscle is always reproducible and invariant. For this reason we fixed most fibres after each experiment, observed $R(f)$ and $O(f)$ and calculated $g(f)$ and $o(f)$ [see Fig. 9a, b for $g(f)$]. Peak–peak amplitude is reduced to $0.1\%L_o$ and 1.6 s (long time course) is spent at each frequency, because (a) fixed muscle is 4–8 times stiffer than a high rigor muscle and (b) better S/N is attained in a longer data collection period. For convenience we

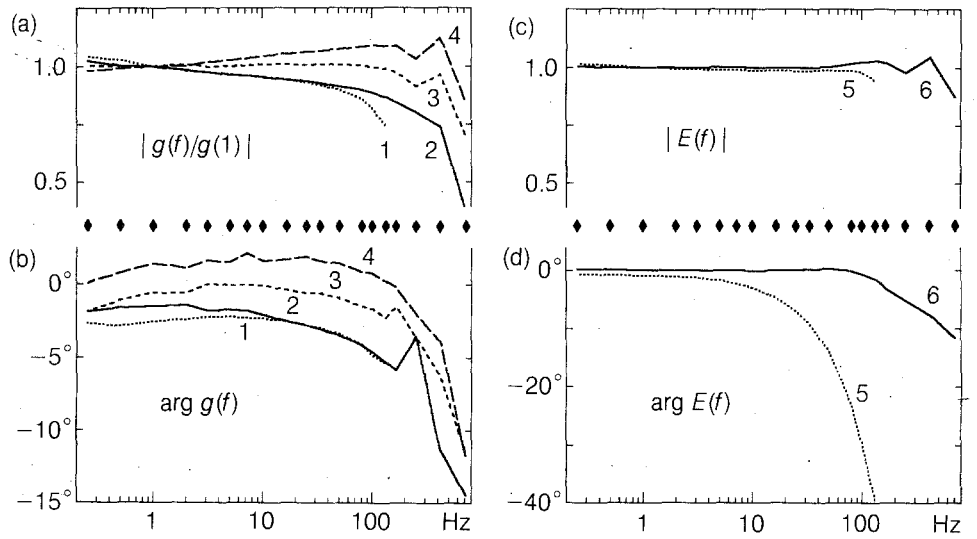

Fig. 9. Calibration functions $g(f)$ (a, b) and $E(f)$ (c, d). (a) and (c) are amplitude plots. (b) and (d) are phase plots. Frequencies at which data are collected are indicated by ♦ and the data points are connected by straight lines. (a) and (b) Curve 1 is for Bionix F100 gauge with plastic clamps; curves 2–4 are for our gauge assembly using Aker's elements: curve 2 (no Vaseline), 3 (moderate amount of Vaseline), 4 (excess Vaseline). (c) and (d) A Clevite Brush carrier amplifier has a sharp roll off (curve 5) than use of a low-noise operational amplifier (BB3500E, curve 6). Curves 2 and 6 are used to create data in Figs. 3 and 5d, while curves 1 and 5 are used to create data in Fig. 5a.

approximate $r(f)$ with a *real* constant. This introduces a trivial error in the correction procedure, since in reality $r(f)$ of a fixed muscle is weakly frequency dependent: $|r(100\,\text{Hz})/r(1\,\text{Hz})| \sim 1.1$, $\arg[r(f)] \sim 3^\circ$ (this can be compensated if necessary). With our most recent equipment (curves 2, 3, 6 in Fig. 9), we are approaching the ideal case: $E(f) \sim 1$, $g(f) \sim g(0) \gg |Y(f)|$, and $o(f) \sim 0$ over the frequency range we routinely use.

In order to judge the integrity of the correction procedure for each day we collected the complex stiffness data of high rigor muscle and compared its corrected form with the standard rigor curves such as those in Fig. 3a, b. If it is visibly different from the standard, as marked by a break in the curves, similarly corrected data is judged unreliable. In this way we obtain quite consistent data even with different muscle clamps, different strain gauges, different amounts of Vaseline in the seal, different fibres, different amplifiers, etc. This method of correction is particularly useful when a strain gauge or an amplifier has a low frequency response.

Appendix 2

Method of data fitting

Complex stiffness data $Y(f)$ [or modulus $Y_M(f)$] is fitted to equation 2 by an expanded version of the least squares method which minimizes D, the sum of modulus squared deviations:

$$D = \sum_f |\Delta Y|^2 = \sum_f \Delta Y^* \Delta Y$$

$$\Delta Y = Y - [H + AX(a) + BX(b) + CX(c)] \tag{8}$$

where $X(a) = fi/(a + fi)$, etc.; * indicates the complex conjugate and the summation is over the N (usually 16) frequencies at which measurements were made. In equation 8, X and Y are experimentally determined *complex* quantities, and a, b, c, A, B, C, H are fitting parameters (*real* quantities). The sign of B (negative) is self-contained for convenience. A complication here is that equation 8 is non-linear with respect to parameters a, b, c, and thus the fitting procedure must be iterative. The fact that complex quantities are used requires some precautions.

It was necessary to invent a technique to find 'best fit' parameters. The following strategy was devised and found satisfactory. (1) The best fit is defined as one which minimizes D. (2) An iteration of linear approximations is used to get sufficiently close to the best fit parameters. (3) The iteration consists of alternately computing least squares magnitude parameters with fixed frequency parameters and computing least squares frequency increments. The fitting is performed as follows.

Step 1. Find from the Nyquist plot the approximate a, b, c, which are the frequencies for the maximum (or the minimum) of the viscous modulus. In Fig. 3c these are 0.7, 17 and 100 Hz respectively.

Step 2. Based on the previously determined a, b, c, find H, A, B, C which minimize D. Since equation 8 is linear with respect to these magnitude parameters, ordinary linear fitting can be applied. In equation 8, by setting

$$\partial D/\partial H = 0, \quad \partial D/\partial A = 0, \quad \partial D/\partial B = 0, \quad \partial D/\partial C = 0$$

$$\begin{pmatrix} H \\ A \\ B \\ C \end{pmatrix} = \begin{pmatrix} N & (1, X(a)) & (1, X(b)) & (1, X(c)) \\ (X(a), 1) & (X(a), X(a)) & (X(a), X(b)) & (X(a), X(c)) \\ (X(b), 1) & (X(b), X(a)) & (X(b), X(b)) & (X(b), X(c)) \\ (X(c), 1) & (X(c), X(a)) & (X(c), X(b)) & (X(c), X(c)) \end{pmatrix}^{-1} \begin{pmatrix} (1, Y) \\ (X(a), Y) \\ (X(b), Y) \\ (X(c), Y) \end{pmatrix}$$

where

$$(X, Z) = \sum_f (X^*Z + XZ^*)/2 = \sum_f R(X^*Z) = \sum_f [R(X)R(Z) + I(X)I(Z)]$$

for given complex numbers X and Z; R, I symbolize real and imaginary parts.

Step 3. Improve previously determined a, b, c by application of a linear expansion:

$$X(a + \Delta a) = X(a) + X'(a)\Delta a; \text{ etc.}$$

where $X'(a) = -fi/(a + fi)^2$. If we replace all Xs in equation 8 with the right hand term of the above equation and the likes, the usual least squares method can be peformed since ΔY is linear with respect to Δa, Δb, Δc. By setting

$$\partial D/\partial \Delta a = 0, \qquad \partial D/\partial \Delta b = 0, \qquad \partial D/\partial \Delta c = 0,$$

we get

$$\begin{pmatrix} \Delta a \\ \Delta b \\ \Delta c \end{pmatrix} = \begin{pmatrix} A(X'(a), X'(a)) & B(X'(a), X'(b)) & C(X'(a), X'(c)) \\ A(X'(b), X'(a)) & B(X'(b), X'(b)) & C(X'(b), X'(c)) \\ A(X'(c), X'(a)) & B(X'(c), X'(b)) & C(X'(c), X'(c)) \end{pmatrix}^{-1} \begin{pmatrix} (X'(a), \Delta Y) \\ (X'(b), \Delta Y) \\ (X'(c), \Delta Y) \end{pmatrix}$$

where $a + \Delta a$, $b + \Delta b$, $c + \Delta c$ are better fit parameters and therefore replace a, b, c. ΔY is defined in equation 8.

Step 4. Repeat steps 2 and 3 until all relative frequency improvements ($|\Delta a/a|$, $|\Delta b/b|$, $|\Delta c/c|$) are less than 0.005. Usually 40 iterations are sufficient to achieve this accuracy and the total computation takes ~ 0.5 min with a Nova 800 computer equipped with a hardware floating point arithmatic unit. If the intial values are within a factor of three, the above iteration converges for good quality data such as shown in Fig. 3. If different initial values within this limit are input, the iteration converges to the same place (this depends on the quality of data).

Calculation of confidence ranges

It is always necessary to assess the reliability of the parameters obtained as a result of fitting because any data can be fitted to any functional form if enough fitting parameters are given. For the fit to give meaningful parameters, the goodness of fit should be sensitive to the values assigned to these parameters. This sensitivity is tested for by calculating the 95% confidence ranges of the fitted parameters according to Fisher's F-statistics. The 'degree of freedom' ($N_{\text{d.f.}}$) appropriate to do this test is:

$$N_{\text{d.f.}} = 2N - (\text{number of fitting parameters}) = 2N - 7$$

where N is the number of frequencies at which data are collected. N is multiplied by two because two points are observed (real and imaginary parts) at each frequency.

The 95% confidence range is evaluated by:

$$D(a,b,c)/D(a_0,b_0,c_0) \leq F(N_{\text{d.f.}})$$

where D is defined in equation 8 as a function of a, b, c. a_0, b_0, c_0 are best fit frequency parameters. The F number is 1.84 for $N_{\text{d.f.}} = 25$. The above inequality indicates that any parameters in this range produce a value of D which does not differ statistically from the minimum value. Since it is impractical to evaluate all the possible ranges, for convenience we calculate the 95% confidence range for each parameter by fixing all the others at their best

values. In the case of the frequency parameter a_0 for instance, we find a which satisfies

$$D(a,b_0,c_0) = F(N_{d.f.})D(a_0,b_0,c_0)$$

Since D function is approximately symmetrical around the best fit value a_0, we get two values for a, the lower and upper limits. We obtained, for the data in Fig. 3, (in Hz) $a = 0.87(0.72 - 1.05)$, $b = 21.9(19.5 - 24.8)$, $c = 83.8(76.5 - 91.9)$ where the 95% confidence ranges are indicated in brackets and plotted in Fig. 3b as horizontal bars along the abscissa. Some other fitted parameters and their confidence ranges have already been published (Kawai *et al.*, 1977; Kawai, 1978, 1979).

Acknowledgements

We are grateful to Dr R. T. Tregear for detailed comments and criticisms in revising the manuscript, to Dr R. H. Abbott for critical reading of the manuscript, to Professor H. Grundfest for useful suggestions during the course of preparation, and to Drs M. Orentlicher and R. N. Cox for valuable comments. This work is supported by grants from NSF (PCM78–08592) and NIH (AM21530, NS05910, NS11766).

References

ABBOTT, R. H. (1972) Comments on the mechanism of force generation in striated muscles. *Nature New Biol.* **239**, 183–6.

ABBOTT, R. H. (1973a) An interpretation of the effects of fiber length and calcium on the mechanical properties of insect flight muscle. *Cold Spring Harb. Symp. quant. Biol.* **37**, 647–54.

ABBOTT, R. H. (1973b) The effects of fibre length and calcium ion concentration on the dynamic response of glycerol extracted insect fibrillar muscle. *J. Physiol., Lond.* **231**, 195–208.

ABBOTT, R. H. & STEIGER, G. J. (1977) Temperature and amplitude dependence of tension transients in glycerinated skeletal and insect fibrillar muscle. *J. Physiol., Lond.* **266**, 13–42.

AMEMIYA, Y., SUGI, H. & HASHIZUME H. (1979) X-ray diffraction studies on the dynamic properties of cross-bridges in skeletal muscle. In *Cross-bridge Mechanism in Muscle Contraction* (edited by SUGI, H. and POLLACK, G. J.), pp. 425–443. Tokyo: University of Tokyo Press.

ARMSTRONG, C. F., HUXLEY, A. F. & JULIAN, F. J. (1966) Oscillatory responses in frog skeletal muscle fibres. *J. Physiol., Lond.* **186**, 26P–27P (abstract).

BENDAT, J. S. & PIERSOL, A. G. (1971) *Random Data: Analysis and Measurement Procedures*. p. 229. New York: Wiley.

BRANDT, P. W., CAPPELL, E. & JEWELL, B. R. (1976) A robust transducer suitable for measuring forces of 1 μN. *J. Physiol., Lond.* **258**, 43–44P (abstract).

BUCHTHAL, F. & KAISER, E. (1951) The rheology of cross striated muscle fibre with particular reference to isotonic conditions. *Dan. Biol. Medd.* **21**, 1–318.

CIVAN, M. M. & PODOLSKY, R. J. (1966) Contraction kinetics of striated muscle fibres following quick change in load. *J. Physiol., Lond.* **184**, 511–34.

EASTWOOD, A. B., WOOD, D. S., BOCK, K. L. & SORENSON, M. M. (1979) Chemically skinned mammalian skeletal muscle. I. The structure of skinned rabbit psoas. *Tiss. Cell* **11**, 553–66.

EDMAN, K. A. P., ELZINGA, G. & NOBLE, M. I. M. (1976) Force enhancement induced by stretch of contracting single isolated muscle fibres of frog. *J. Physiol., Lond.* **258**, 95–6P (abstract).

FENN, F. O. (1923) A quantitative comparison between the energy liberated and the work performed by the isolated sartorius muscle of the frog. *J. Physiol., Lond.* **58**, 175–203.

FORD, L. E., HUXLEY, A. F. & SIMMONS, R. M. (1977) Tension responses to sudden length change in stimulated frog muscle fibres near slack length. *J. Physiol., Lond.* **269**, 441–515.

GASSER, H. S. & HILL, A. V. (1924) The dynamics of muscular contraction. *Proc. Roy. Soc., Series B* **96**, 398–437.

GIRARDIER, L., REUBEN, J. P., BRANDT, P. W. & GRUNDFEST, H. (1963) Evidence for anion-permselective membrane in crayfish muscle fibers and its possible role in excitation–contraction coupling. *J. gen. Physiol.* **47**, 189–214.

HEINL, P., KUHN, H. J. & RÜEGG, J. C. (1974) Tension responses to quick length changes of glycerinated skeletal muscle fibers from the frog and tortoise. *J. Physiol., Lond.* **237**, 243–58.

HILL, A. V. (1953) The mechanics of active muscle. *Proc. Roy. Soc., Series B* **141**, 104–17.

HILL, L. (1977) A-band length, striation spacing and tension change on stretch of active muscle. *J. Physiol., Lond.* **266**, 677–85.

HILL, T. L. (1974) Theoretical formalism for the sliding filament model of contraction of striated muscle. Part I. *Prog. Biosphys. molec. Biol.* **28**, 267–340.

HILL, T. L., EISENBERG, E., CHEN, Y-D. & PODOLSKY, R. J., (1975) Some self-consistent two-state sliding filament models of muscle contraction. *Biophys. J.* **15**, 335–72.

HUXLEY, A. F. (1957) Muscle structure and theories of contraction. *Prog. Biophys.* **7**, 255–318.

HUXLEY, A. F. (1974) Muscular contraction. *J. Physiol., Lond.* **243**, 1–43.

HUXLEY, A. F. & SIMMONS, R. M. (1971) Proposed mechanism of force generation in striated muscle. *Nature, Lond.* **233**, 533–8.

HUXLEY, A. F. & SIMMONS, R. M. (1973) Mechanical transients and the origin of muscular force. *Cold Spring Harb. Symp. quant. Biol.* **37**, 669–80.

JULIAN, F. J. (1969) Activation in a skeletal muscle contraction model with a modification for insect fibrillar muscle. *Biophys. J.* **9**, 547–70.

JULIAN, F. J., SOLLINS, K. R. & SOLLINS, M. R. (1974) A model for the transient and steady-state mechanical behavior of contracting muscle. *Biophys. J.* **14**, 546–62.

KAWAI, M. (1978) Head rotation or dissociation? A study of exponential rate processes in chemically skinned rabbit muscle fibers when MgATP concentration is changed. *Biophys. J.* **22**, 97–103.

KAWAI, M. (1979) Effect of MgATP on cross-bridge kinetics in chemically skinned rabbit psoas fibers as measured by sinusoidal analysis technique. In *Cross-bridge Mechanism in Muscle Contraction* (edited by SUGI, H. and POLLACK, G. H.), pp. 149–169. Tokyo: University of Tokyo Press.

KAWAI, M. & BRANDT, P. W. (1975) Complex stiffness of activated single crayfish muscle fibers. *Biophys. J.* **15**, 154a (abstract).

KAWAI, M. & BRANDT, P. W. (1976) Two rigor states in skinned crayfish single muscle fibers. *J. gen. Physiol.* **68**, 267–80.

KAWAI, M. & BRANDT, P. W. (1979) Effect of ATP buffer concentration on the mechanical rate constants in chemically skinned rabbit psoas fibers. *Biophys. J.* **25**, 270a (abstract).

KAWAI, M. & ORENTLICHER, M. (1976) Effect of inorganic phosphate (Pi), substrate (MgATP), and excess ATP on complex stiffness of skinned crayfish muscle fibers and glycerinated rabbit psoas muscle bundles. *Biophys. J.* **16**, 152a (abstract).

KAWAI, M., BRANDT, P. W. & ORENTLICHER, M. (1977) Dependence of energy transduction in intact skeletal muscles on the time in tension. *Biophys. J.* **18**, 161–72.

LYMN, R. W. & TAYLOR, E. W. (1971) The mechnism of adenosine triphosphate hydrolysis by actomyosin. *Biochemistry* **10**, 4617–24.

MACHIN, K. E. (1964) Feedback theory and its application to biological systems. *Symp. Soc. exp. Biol.* **18**, 421–45.

MACHIN, K. E. & PRINGLE, J. W. S. (1959) The physiology of insect flight muscle. II. The mechanical properties of a beetle flight muscle. *Proc. Roy. Soc., Series B* **151**, 204–25.

PODOLSKY, R. J. (1960) Kinetics of muscular contraction: the approach to the steady state. *Nature, Lond.* **188**, 666–8.

PODOLSKY, R. J. & NOLAN, A. C. (1973) Muscle contraction transients, cross-bridge kinetics, and the Fenn effect. *Cold Spring Harb. Symp. quant. Biol.* **37**, 661–8.

PODOLSKY, R. J., GULATI, J. & NOLAN, A. C. (1974) Contraction transients of skinned muscle fibers. *Proc. natn. Acad. Sci.* **71**, 1516–9.

PRINGLE, J. W. S. (1967) The contractile mechanism of insect fibrillar muscle. *Prog. Biophys. molec. Biol.* **17**, 1–60.

PRINGLE, F. R. S. (1978) Stretch activation of muscle: function and mechanism. *Proc. Roy. Soc. Lond., Series B* **201**, 107–30.

PYBUS, J. & TREGEAR, R. T. (1975) The relationship of adenosine triphosphatase activity to tension and power output of insect flight muscle. *J. Physiol., Lond.* **247**, 71–89.

RACK, P. M. H. (1966) The behavior of a mammalian muscle during sinusoidal stretching. *J. Physiol., Lond.* **183**, 1–14.

REUBEN, J. P., BRANDT, P. W. & GRUNDFEST, H. (1967) Tension evoked in skinned crayfish muscle fibers by anions, pH, and drugs. *J. gen. Physiol.* **50**, 2501 (abstract).

REUBEN, J. P., BRANDT, P. W., BERMAN, M. & GRUNDFEST, H. (1971) Regulation of tension in the skinned crayfish muscle fiber. *J. gen. Physiol.* **57**, 385–407.

REUBEN, J. P., WOOD, D. S. & EASTWOOD, A. B. (1977) Adaptation of single fiber techniques for the study of human muscle. In *Pathogenesis of Human Muscular Dystrophies* (edited by RAWLAND, L. P.), pp. 259–269. Amsterdam: Excerpta Medica.

RÜEGG, J. C. & TREGEAR, R. T. (1966) Mechanical factors affecting the ATPase activity of glycerol-extracted fibres of insect fibrillar flight muscle. *Proc. Roy. Soc., Series B* **165**, 497–512.

SAEKI, Y., SAGAWA, K. & SUGA, H. (1978) Dynamic stiffness of cat heart muscle in Ba^{2+}-induced contracture. *Circulation Res.* **42**, 324–33.

STEIGER, G. J. (1971) Stretch activation and myogenic oscillation of isolated contractile structures of heart muscle. *Pflügers Arch. Eur. J. Physiol.* **330**, 347–61.

STEIGER, G. J. & RÜEGG, J. C. (1969) Energetics and 'efficiency' in the isolated contractile machinery of an insect fibrillar muscle at various frequencies of oscillation. *Pflügers Arch. Eur. J. Physiol.* **307**, 1–21.

STEIN, L. A., SCHWARZ, R. P., CHOCK, P. B. & EISENBERG, E. (1979) Mechanism of actomyosin adenosine triphosphatase. Evidence that adenosine 5'-triphosphate hydrolysis can occur without dissociation of the actomyosin complex. *Biochemistry* **18**, 3895–909.

SUGI, H. (1972) Tension changes during and after stretch in frog muscle fibres. *J. Physiol., Lond.* **225**, 237–53.

SUGI, H. (1979) The origin of the series elasticity in striated muscle fibers. In *Cross-bridge Mechanism in Muscle Contraction* (edited by SUGI, H. and POLLACK, G. H.), pp. 85–102. Tokyo: University of Tokyo Press.

SUGI, H. & TAMEYASU, T. (1979) The origin of the instantaneous elasticity in single frog muscle fibers. *Experimentia* **35**, 227–8.

THORSON, J. W. & WHITE, D. C. S. (1969) Distributed representations for actomyosin interaction in the oscillatory contraction of muscle. *Biophys. J.* **9**, 360–90.

TRENTHAM, D. R., ECCLESTON, J. F. & BAGSHAW, C. R. (1976) Kinetic analysis of ATPase mechanisms. *Q. Rev. Biophys.* **9**, 217–81.

WHITE, D. C. S. & THORSON, J. (1972) Phosphate starvation and the nonlinear dynamics of insect fibrillar flight muscle. *J. gen. Physiol.* **60**, 307–36.

WHITE, D. C. S. & THORSON, J. (1973) The kinetics of muscle contraction. *Prog. Biosphys. molec. Biol.* **27**, 173–255.

WOOD, D. S., ZOLLMAN, J., REUBEN, J. P. & BRANDT, P. W. (1975) Human skeletal muscle: properties of the 'chemically skinned' fiber. *Science, N.Y.* **197**, 1075–6.